

# Nanoscale

Accepted Manuscript



This is an *Accepted Manuscript*, which has been through the Royal Society of Chemistry peer review process and has been accepted for publication.

*Accepted Manuscripts* are published online shortly after acceptance, before technical editing, formatting and proof reading. Using this free service, authors can make their results available to the community, in citable form, before we publish the edited article. We will replace this *Accepted Manuscript* with the edited and formatted *Advance Article* as soon as it is available.

You can find more information about *Accepted Manuscripts* in the [Information for Authors](#).

Please note that technical editing may introduce minor changes to the text and/or graphics, which may alter content. The journal's standard [Terms & Conditions](#) and the [Ethical guidelines](#) still apply. In no event shall the Royal Society of Chemistry be held responsible for any errors or omissions in this *Accepted Manuscript* or any consequences arising from the use of any information it contains.

Cite this: DOI: 10.1039/c0xx00000x

www.rsc.org/xxxxxx

PAPER

# Radionuclide $^{131}\text{I}$ -labeled multifunctional dendrimers for targeted SPECT imaging and radiotherapy of tumors†

Jingyi Zhu,<sup>1a</sup> Lingzhou Zhao,<sup>1b</sup> Yongjun Cheng,<sup>b</sup> Zhijuan Xiong,<sup>c</sup> Yueqin Tang,<sup>d</sup> Mingwu Shen,<sup>c</sup> Jinhua Zhao<sup>\*b</sup> and Xiangyang Shi<sup>\*a,c</sup>Received (in XXX, XXX) Xth XXXXXXXXXX 20XX, Accepted Xth XXXXXXXXXX 20XX  
DOI: 10.1039/b000000x

We report the synthesis, characterization, and utilization of radioactive  $^{131}\text{I}$ -labeled multifunctional dendrimers for targeted single-photon emission computed tomography (SPECT) imaging and radiotherapy of tumors. In this study, amine-terminated poly(amidoamine) dendrimers of generation 5 (G5.NH<sub>2</sub>) were sequentially modified with 3-(4'-hydroxyphenyl)propionic acid-OSu (HPAO) and folic acid (FA) linked with polyethylene glycol (PEG), followed by acetylation modification of the dendrimer remaining surface amines and labeling of radioactive iodine-131 ( $^{131}\text{I}$ ). The generated multifunctional  $^{131}\text{I}$ -G5.NHAc-HPAO-PEG-FA dendrimers were characterized *via* different methods. We show that prior to the  $^{131}\text{I}$  labeling, the G5.NHAc-HPAO-PEG-FA dendrimers conjugated with approximately 9.4 HPAO moieties per dendrimer are noncytotoxic at a concentration up to 20  $\mu\text{M}$  and are able to target cancer cells overexpressing FA receptors (FAR) thanks to the modified FA ligands. In the presence of phenol group, radioactive  $^{131}\text{I}$  is able to be efficiently labeled onto the dendrimer platform with good stability and high radiochemical purity, and render the platform with an ability for targeted SPECT imaging and radiotherapy of an FAR-overexpressing xenografted tumor model *in vivo*. The designed strategy to use facile dendrimer nanotechnology may be used to form various radioactive theranostic nanoplatfoms for targeted SPECT imaging and radiotherapy of different types of cancer.

## Introduction

Nuclear medicine makes a significant contribution in the area of healthcare sciences, particularly in the imaging and therapy of cancer and cardiovascular diseases.<sup>1-7</sup> As one of the most important nuclear medical imaging techniques, single-photon emission computed tomography (SPECT) has the advantages of high sensitivity and capacity for functional imaging.<sup>8-13</sup> For SPECT imaging, radionuclides such as technetium-99 ( $^{99\text{m}}\text{Tc}$ ), indium-111 ( $^{111}\text{In}$ ), gallium-67 ( $^{67}\text{Ga}$ ), thallium-201 ( $^{201}\text{Tl}$ ), and iodine-131 ( $^{131}\text{I}$ ) are generally used.<sup>9, 14, 15</sup> On the other hand, radiotherapy has been considered as a sensitive therapeutic approach, possessing high therapeutic efficiency in the presence of radiopharmaceuticals,<sup>16, 17</sup> since the therapeutic effect is based on the absorption of alpha ( $\alpha$ ) or beta ( $\beta$ ) radiation energy emitted by the radionuclide. Therefore, selection of an appropriate radionuclide enables simultaneous SPECT imaging and radiotherapy, which is important for theranostics of cancer. Among many used radionuclides,  $^{131}\text{I}$  has attracted a great deal of interest due to its relative long half-life ( $t_{1/2} = 8.01$  days) and both  $\gamma$ -ray emission (364 keV, 81.7%) for SPECT imaging and  $\beta$ -ray emission (0.606 MeV, 89.9%) for radiotherapy, which is important for theranostic applications.<sup>18-20</sup> Due to the non-specificity, short circulation time *in vivo*, and low accumulation at the disease site,<sup>3, 21</sup> free radionuclides are unable to achieve

effective nuclear imaging and radiotherapy of diseases. With the advances of nanotechnology, it is essential to design various nanoscale carriers for selective delivery of radionuclides in order to improve the efficiency of cancer diagnosis and therapy.

Poly(amidoamine) (PAMAM) dendrimers have been widely used as a platform for cancer imaging<sup>22-31</sup> and therapy.<sup>32-34</sup> Through the use of the versatile dendrimer nanotechnology,<sup>35</sup> targeting ligands,<sup>22, 37, 38</sup> therapeutic drug molecules, and imaging agents can be loaded onto the dendrimer platform for targeted cancer imaging and therapy.<sup>27, 28, 30, 32, 35, 36, 39-41</sup> For instance anticancer drug-conjugated generation 5 (G5) PAMAM dendrimers with gold nanoparticles entrapped within their interiors are able to be used as a platform for targeted computed tomography imaging and chemotherapy of cancer cells *in vitro* and *in vivo*.<sup>42</sup> Likewise, multivalent attachment of chelators for radionuclide labeling onto dendrimers is also possible, allowing for the design of dendrimer-based radiopharmaceuticals for SPECT imaging applications.<sup>43-49</sup> For instance, G5 PAMAM dendrimers were used as a platform to link multiple diethylenetriaminepentaacetic acid (DTPA) chelators for  $^{99\text{m}}\text{Tc}$  labeling and folic acid (FA) for targeting FA receptor (FAR)-overexpressing cancer cells.<sup>43</sup> However, to the best of our knowledge, there is no study up to now demonstrating the utilization of dendrimers as a unique nanoplatfom to load radiopharmaceuticals for both SPECT imaging and radiotherapy

of cancer.

Inspired by the property of radioactive  $^{131}\text{I}$  that can be used for both SPECT imaging and radiotherapy and the versatile dendrimer nanotechnology, here we report a dendrimer-based theranostic nanoplatfrom that can be used for targeted tumor SPECT imaging and radiotherapy. In this work, G5 PAMAM dendrimers with amine termini (G5.NH<sub>2</sub>) were sequentially conjugated with 3-(4'-hydroxyphenyl)propionic acid-OSu (HPAO) and FA-linked with polyethylene glycol (PEG), followed by acetylating the dendrimer remaining surface amines and labeling of  $^{131}\text{I}$  with the HPAO phenol group (Figure 1). The formed multifunctional G5.NHAc-HPAO-PEG-FA dendrimers before and after  $^{131}\text{I}$  labeling were characterized *via* different methods. *In vitro* cell viability test was used to evaluate the cytotoxicity of the G5.NHAc-HPAO-PEG-FA dendrimers. The binding specificity of the G5.NHAc-HPAO-PEG-FA dendrimers to FAR-overexpressing cancer cells was evaluated *via* flow cytometry and confocal microscopy *in vitro*. The radiochemical purity of the  $^{131}\text{I}$ -G5.NHAc-HPAO-PEG-FA dendrimers at different time points was tested to prove the stability of the  $^{131}\text{I}$  labeling. Finally, the formed  $^{131}\text{I}$ -G5.NHAc-HPAO-PEG-FA dendrimers were used as a platform for targeted SPECT imaging and radiotherapy of a xenografted FAR-overexpressing tumor model *in vivo*. To the best of our knowledge, this work is the first to report the development of  $^{131}\text{I}$ -labeled dendrimer nanoplatfrom for targeted tumor SPECT imaging and radiotherapy.

## Experimental

### Materials

G5.NH<sub>2</sub> PAMAM dendrimers with ethylenediamine core having a polydispersity index less than 1.08 (theoretical Mw = 28 826, diameter = 5.4 nm<sup>50</sup>) were provided from Dendritech (Midland, MI). HPAO, chloramine-T trihydrate (ch-T), potassium iodide (KI), and sodium metabisulfite (Na<sub>2</sub>S<sub>2</sub>O<sub>5</sub>) were supplied by J&K China Chemical Ltd. (Shanghai, China). PEG having one amine end group and the other carboxyl end group (NH<sub>2</sub>-PEG-COOH, Mw = 5 000) and PEG monomethyl ether with carboxyl end group (*m*PEG-COOH, Mw = 5 000) were from Shanghai Yanyi Biotechnology Corporation (Shanghai, China). Na $^{131}\text{I}$  solution was purchased from Shanghai GMS Pharmaceutical Co., Ltd (Shanghai, China). 3-(4,5-Dimethylthiazol-2-yl)-2,5-diphenyltetrazolium bromide (MTT), FA, 1-ethyl-3-(3-dimethylaminopropyl) carbodiimide hydrochloride (EDC), and all other chemicals and reagents were supplied from Aldrich (St. Louis, MO). Disposable PD-10 desalting columns were procured from GE Pharmacia (GE Inc., Fairfield, CT). C6 cells (a rat glioma cell line) were obtained from Institute of Biochemistry and Cell Biology (the Chinese Academy of Sciences, Shanghai, China). Dulbecco's Modified Eagle's Medium (DMEM), fetal bovine serum (FBS), penicillin, and streptomycin were obtained from Hangzhou Jinuo Biomedical Technology (Hangzhou, China). Water used in all experiments was subjected to purification using a Milli-Q Plus 185 water purification system (Millipore, Bedford, MA) and has a resistivity higher than 18 MΩ·cm. Regenerated cellulose dialysis membranes (MWCO = 14 000 and 1 000) were purchased from Fisher (Pittsburgh, PA).

### Synthesis of the G5.NHAc-HPAO-PEG-FA dendrimers

To synthesize the G5.NHAc-HPAO-PEG-FA dendrimers, PEGylated FA with carboxyl end group (FA-PEG-COOH) was first synthesized according to protocols described in the literature.<sup>42</sup> G5.NH<sub>2</sub> (10.0 mg, in 5 mL DMSO) was reacted with 12 molar equivalents of HPAO (1.21 mg, 5 mL in DMSO) under stirring. After 24 h, the formed raw product of G5.NH<sub>2</sub>-HPAO was subsequently reacted with the EDC-activated FA-PEG-COOH. In brief, FA-PEG-COOH (100.95 mg, in 5.0 mL DMSO), having 50 molar equivalents of G5.NH<sub>2</sub> was activated with EDC (73.7 mg, in 5.0 mL DMSO), and reacted with the raw product of G5.NH<sub>2</sub>-HPAO under stirring for 3 days to get the raw product of G5.NH<sub>2</sub>-HPAO-PEG-FA conjugates. The raw G5.NH<sub>2</sub>-HPAO-PEG-FA conjugates were subjected to an acetylation reaction and purified *via* dialysis according to the literature.<sup>42</sup> This led to the formation of the G5.NHAc-HPAO-PEG-FA dendrimers. For comparison, G5.NHAc-HPAO-*m*PEG dendrimers without FA were also synthesized using *m*PEG-COOH and characterized.

### Formation of the $^{131}\text{I}$ -G5.NHAc-HPAO-PEG-FA dendrimers

Radioactive  $^{131}\text{I}$  labeling of the G5.NHAc-HPAO-PEG-FA dendrimers was performed according to protocols described in the literature.<sup>51, 52</sup> In a typical experiment, G5.NHAc-HPAO-PEG-FA (200 μg) and ch-T (100 μg) co-dissolved in 200 μL PBS (0.1 M, PH = 7.2-7.4) were added with sterile Na $^{131}\text{I}$  solution (185-370 MBq, 0.5-1 mL) immediately with continuous mixing. The reaction mixture was incubated at room temperature for 2 min. Then Na<sub>2</sub>S<sub>2</sub>O<sub>5</sub> (100 μg) was added to terminate the reaction. After that, PD-10 desalting columns were used to purify the  $^{131}\text{I}$ -labeled G5.NHAc-HPAO-PEG-FA ( $^{131}\text{I}$ -G5.NHAc-HPAO-PEG-FA) dendrimers. The radioactivity of each aliquot tube was measured by CRC-15R radioisotope dose calibrator (Capintec, Inc., Ramsey, NJ).

### Characterization techniques

$^1\text{H}$  NMR spectra were collected using Bruker AV-400 NMR spectrometer. Samples before  $^{131}\text{I}$  labeling were dissolved in D<sub>2</sub>O before measurements. The radiochemical purity of the  $^{131}\text{I}$ -G5.NHAc-HPAO-PEG-FA dendrimers was analyzed by instant thin-layer chromatography (ITLC) using silica gel-coated fiber glass slides (Macherey-Nagel, GmbH & Co. KG, Düren Germany) and saline as the mobile phase. The slides were scanned and assessed by Thin-Layer Chromatogram Scanner (Bioscan Inc., Tucson, AZ).

### *In vitro* stability study

The radiolabeling stability of the  $^{131}\text{I}$ -G5.NHAc-HPAO-PEG-FA dendrimers *in vitro* was evaluated by ITLC.<sup>51</sup> In brief, the  $^{131}\text{I}$ -G5.NHAc-HPAO-PEG-FA dendrimers (100 μL, 18.5 MBq) were mixed with 1 mL PBS. ITLC was carried out to assess the radiochemical purity of the  $^{131}\text{I}$ -G5.NHAc-HPAO-PEG-FA dendrimers after incubation at room temperature for 0 h, 1 h, 3 h, and 27 h, respectively.

### Cell culture

C6 cells were regularly cultured at 37 °C in a 5% CO<sub>2</sub> incubator using DMEM that was supplemented with 10% FBS, 100 U/mL penicillin, and 100 U/mL streptomycin. The C6 cells grown in FA-free medium had high-level FAR expression (denoted as C6-HFAR), while the cells grown in FA-containing medium (2.5 μM

FA) for 24 h or longer had low-level FAR expression (denoted as C6-LFAR).

#### ***In vitro* cytotoxicity assay**

MTT assay was used to evaluate the cytotoxicity of the G5.NHAc-HPAO-PEG-FA dendrimers *in vitro* using C6-HFAR cells. The assay was performed according to the literature.<sup>53</sup> After treatment with the G5.NHAc-HPAO-PEG-FA dendrimers with different concentrations for 24 h, the cell morphology was observed using a Leica DM IL LED inverted phase contrast microscope. The magnification was set at 200 × for all samples.

#### **Flow cytometry analysis**

In order to evaluate the targeting specificity of the G5.NHAc-HPAO-PEG-FA dendrimers *via* flow cytometry, we conjugated fluorescein isothiocyanate (FI) onto the G5 dendrimers according to our previous work<sup>32</sup> to form the G5.NHAc-FI-HPAO-PEG-FA dendrimers with the same modifications of HPAO, PEG-FA, and acetylation to those of the G5.NHAc-HPAO-PEG-FA dendrimers without FI. Both C6-HFAR and C6-LFAR cells were seeded in 12-well cell culture plates (at a density of  $2 \times 10^5$  cells per well) one day before the experiment, then the cells were washed 4 times with serum-free FA-deficient DMEM and cultured with the fresh FA-deficient DMEM containing G5.NHAc-FI-HPAO-PEG-FA or G5.NHAc-FI-HPAO-*m*PEG dendrimers at a concentration of 1000 nM. After 2 h incubation, the cells were lifted *via* trypsinization, resuspended in PBS (containing 0.1% bovine serum albumin), and analyzed using a Becton Dickinson FACScan analyzer.

#### **Confocal microscopy**

The specific uptake of the G5.NHAc-FI-HPAO-PEG-FA dendrimers by C6-HFAR cells was confirmed by confocal microscopy (Carl Zeiss LSM 700, Jena, Germany) according to our previous reports.<sup>54,55</sup>

#### **Targeted SPECT imaging of a xenografted tumor model *in vivo***

Animal experiments were performed after approval by the ethical committee of Shanghai General Hospital. Female 4- to 6-week old BALB/c nude mice (22-26 g, Shanghai Slac Laboratory Animal Center, Shanghai, China) were subcutaneously injected with  $2 \times 10^6$  C6-HFAR cells/mouse in the right side of their flank to establish the tumor model. The mice were randomly divided into the experimental and control groups. Furthermore, in order to reduce the thyroid uptake of the <sup>131</sup>I-labeled dendrimers, all nude mice were fed with 1% potassium iodide (in drinking water) for 7 days before the SPECT imaging experiment. When the tumor volume reached 0.5-1.2 cm<sup>3</sup> at about 3 weeks postinjection, a PBS solution of the <sup>131</sup>I-G5.NHAc-HPAO-PEG-FA dendrimers ( $[^{131}\text{I}] = 92.5 \text{ MBq/mL}$ , 200 μL) was intravenously delivered to the mice *via* the tail vein. For comparison, nontargeted <sup>131</sup>I-G5.NHAc-HPAO-*m*PEG dendrimers without FA were also administered at the same dose. All mice were anesthetized with pentobarbital sodium (40 mg/kg) before SPECT imaging.

SPECT imaging was performed with Infinia GE SPECT equipped with Xeleris Work Station and High Energy General Purpose detector (GE Inc., Fairfield, CT). SPECT images were acquired at 2 min, 30 min, 1 h, 2 h, 3 h, 4 h, 6 h, 16 h, and 24 h

postinjection. At 6 h and 24 h postinjection, one mouse was sacrificed by cervical dislocation in different experimental groups, respectively. Major organs and tumors were collected and their radioactivity ratios were calculated by analyzing the regions of interests.

#### **Targeted tumor radiotherapy *in vivo***

The tumor mice described above were intravenously injected with a solution of the <sup>131</sup>I-G5.NHAc-HPAO-*m*PEG or <sup>131</sup>I-G5.NHAc-HPAO-PEG-FA dendrimers ( $[^{131}\text{I}] = 37 \text{ MBq/mL}$ , 200 μL, for each mouse) *via* the tail vein every third day. Mice were also injected with saline (200 μL), Na<sup>131</sup>I (200 μL), G5.NHAc-HPAO-*m*PEG dendrimers (200 μL) with the same concentration of the <sup>131</sup>I-G5.NHAc-HPAO-*m*PEG dendrimers, and G5.NHAc-HPAO-PEG-FA dendrimers (200 μL) with the same concentration of the <sup>131</sup>I-G5.NHAc-HPAO-PEG-FA dendrimers every third day for comparison. The tumor inhibition efficacy was evaluated according to protocols described in our previous work.<sup>42</sup> Mice treated with saline, Na<sup>131</sup>I, G5.NHAc-HPAO-*m*PEG, G5.NHAc-HPAO-PEG-FA, <sup>131</sup>I-G5.NHAc-HPAO-*m*PEG, and <sup>131</sup>I-G5.NHAc-HPAO-PEG-FA were sacrificed after 21 days' treatment, then the tumors and the major organs (the heart, liver, spleen, lung, and kidney) were harvested, treated, sectioned, hematoxylin and eosin (H&E) stained, and observed using protocols described in our previous work.<sup>42</sup> The apoptosis on tumor tissues was assessed *via* a terminal deoxynucleotidyl transferase dUTP nick end labeling (TUNEL) method according to the protocol described in our previous work.<sup>42</sup>

#### **Statistical analysis**

The significance of the experimental data was evaluated *via* one-way analysis of variance (ANOVA) or analysis of covariance (ANCOVA) statistical analysis. A value of 0.05 was used as the significance level, and the data were presented with (\*) for  $p < 0.05$ , (\*\*) for  $p < 0.01$ , and (\*\*\*) for  $p < 0.001$ , respectively. Additional experimental details can be seen in Electronic Supplementary Information (ESI).

## **Results and discussion**

### **Synthesis and characterization of the <sup>131</sup>I-G5.NHAc-HPAO-PEG-FA dendrimers**

As schematically illustrated in Figure 1, amine-terminated G5 PAMAM dendrimers were used as a platform to sequentially conjugate with HPAO (for <sup>131</sup>I labeling<sup>52</sup>) and PEGylated FA (for tumor targeting), followed by acetylating the dendrimer remaining terminal amines and labeling of <sup>131</sup>I. The former multifunctional <sup>131</sup>I-G5.NHAc-HPAO-PEG-FA dendrimers were characterized *via* different techniques.

First, the conjugation of HPAO with the G5.NH<sub>2</sub> dendrimers was first characterized by <sup>1</sup>H NMR spectroscopy (Figure S1, electronic supplementary information, ESI). By integration of the characteristic proton peaks at 6.6 ppm and 6.9 ppm associated with the phenol of HPAO, the practical number of HPAO moieties attached to each dendrimer was estimated to be 9.4. Then, PEGylated FA (0.6 FA moieties attached to each PEG) characterized *via* <sup>1</sup>H NMR, Figure S2, ESI) was next conjugated onto the surface of G5 dendrimers. Through the comparison of the NMR integration between the G5 -CH<sub>2</sub>- protons and the

CH<sub>2</sub>- protons of the PEG, the number of PEG-FA modified onto each G5 dendrimer was measured to be 34.9 (Figure S3, ESI). Hence, the practical number of FA moieties attached to each G5 dendrimer can be calculated to be 20. The control device of the G5.NHAc-HPAO-*m*PEG dendrimers (Figure S4, ESI) without FA was characterized to have the comparable number of PEG moieties per G5 dendrimer to that of the G5.NHAc-HPAO-PEG-FA dendrimer.

Then the labeling of <sup>131</sup>I with the G5.NHAc-HPAO-PEG-FA dendrimers was performed *via* the chloramines T method with the optimum labeling yield. Quality control tests using ITLC reveal that the mean radiochemical purity of the <sup>131</sup>I-G5.NHAc-HPAO-PEG-FA dendrimer is 97.7% ± 0.7%.

#### Stability of the <sup>131</sup>I-G5.NHAc-HPAO-PEG-FA dendrimers

The radio stability of the <sup>131</sup>I-G5.NHAc-HPAO-PEG-FA dendrimers needs to be first addressed. We tested the radiochemical purity of the <sup>131</sup>I-labeled G5.NHAc-HPAO-PEG-FA dendrimers to check whether the <sup>131</sup>I was separated from the dendrimer platform or not (Figure S5, ESI). The ITLC curves of the <sup>131</sup>I-G5.NHAc-HPAO-PEG-FA dendrimers show a single peak (Rf value = 0.1-0.2), demonstrating that free <sup>131</sup>I was effectively removed through purification. As a control, free Na<sup>131</sup>I has a different Rf value (0.8-0.9) in the ITLC chromatogram. It can be seen that the <sup>131</sup>I-G5.NHAc-HPAO-PEG-FA dendrimers display acceptable stability *in vitro* for at least 27 h when they were stored at room temperature in PBS. Quantitative analysis shows that the radiochemical purity of the product is > 90% at different time intervals (Table S1, ESI). These results demonstrate that the <sup>131</sup>I-G5.NHAc-HPAO-PEG-FA dendrimers possess good radio stability, which is essential for their further SPECT imaging and radiotherapy applications.

#### Cytotoxicity assay

Prior to the labeling of <sup>131</sup>I, it's essential to investigate the cytocompatibility of the formed G5.NHAc-HPAO-PEG-FA dendrimers. The cytotoxicity of the G5.NHAc-HPAO-PEG-FA dendrimers was evaluated by MTT assay of the viability of C6 cells (Figure 2). It is clear that the G5.NHAc-HPAO-PEG-FA dendrimers do not exhibit appreciable cytotoxicity to the C6 cells at a concentration up to 20 μM when compared with the C6 cells treated with PBS (p > 0.05). The cytocompatibility of the G5.NHAc-HPAO-PEG-FA dendrimers was then confirmed *via* microscopic observation of the cells treated with the G5.NHAc-HPAO-PEG-FA dendrimers (Figure S6, ESI). It is clear that the treatment of the G5.NHAc-HPAO-PEG-FA dendrimers at a concentration up to 20 μM does not induce any significant morphology changes of the cells, similar to the control cells treated with PBS. These results corroborate the MTT assay data, demonstrating the excellent cytocompatibility of the G5.NHAc-HPAO-PEG-FA dendrimers.

#### Targeting specificity of the G5.NHAc-HPAO-PEG-FA dendrimers

A range of human carcinomas have been known to overexpress FAR.<sup>56, 57</sup> Here, we used the FI-conjugated dendrimers to test the targeting specificity of the G5.NHAc-FI-HPAO-PEG-FA dendrimers to FAR-overexpressing C6 cells *via* flow cytometry and confocal microscopy. The number of FI moieties conjugated

onto each G5 dendrimer for either targeted G5.NHAc-FI-HPAO-PEG-FA or nontargeted G5.NHAc-FI-HPAO-*m*PEG dendrimer was estimated to be 5.6 and 5.4, respectively (Figure S7, ESI).

This ensures the reasonable comparison of the dendrimer conjugates in terms of the fluorescence intensity measurements. Flow cytometric analysis of C6 cells (Figure S8, ESI) reveals that after 2 h incubation with the G5.NHAc-FI-HPAO-PEG-FA dendrimers, the C6-HFAR cells display significant fluorescence enhancement than the C6-LFAR cells (Figures S8e, S8d, and S8f, ESI). In contrast, both C6-HFAR and C6-LFAR cells treated with the nontargeted G5.NHAc-FI-HPAO-*m*PEG dendrimers without FA do not exhibit appreciably enhanced fluorescence intensity (Figures S8b, S8c, and S8f, ESI), instead display slightly higher fluorescence intensity than the C6-HFAR cells treated with PBS (Figure S8a, ESI). This suggests that the binding of the G5.NHAc-FI-HPAO-PEG-FA dendrimers with C6-HFAR cells is quite specific thanks to the FAR-mediated targeting pathway.<sup>58, 59</sup> The slightly higher fluorescence intensity of the C6-HFAR cells treated with the G5.NHAc-FI-HPAO-*m*PEG dendrimers and C6-LFAR cells treated with either the G5.NHAc-FI-HPAO-*m*PEG dendrimers or the G5.NHAc-FI-HPAO-PEG-FA dendrimers may be due to the non-specific cellular uptake of the particles through two distinct mechanisms of phagocytosis and diffusion *via* cell walls.<sup>28, 29</sup>

The conjugated FI moiety onto the dendrimers also afforded the cellular uptake of the particles to be visualized *via* confocal microscopy (Figure 3). After 2 h incubation with the G5.NHAc-FI-HPAO-PEG-FA dendrimers, only C6-HFAR cells exhibit prominent fluorescence signals that are associated with the specific binding and cellular internalization of the particles. In sharp contrast, the C6-LFAR cells treated with the G5.NHAc-FI-HPAO-PEG-FA dendrimers and both C6-LFAR and C6-HFAR cells treated with the G5.NHAc-FI-HPAO-*m*PEG dendrimers do not have appreciable fluorescence signals under similar microscopic conditions. These results suggest that the FA modification renders the dendrimers to be specifically uptaken by the C6-HFAR cells. Taken together, our results suggest that the G5.NHAc-FI-HPAO-PEG-FA dendrimers can be specifically delivered to the FAR-overexpressing cancer cells *via* receptor-mediated binding and endocytosis pathway.

#### Targeted SPECT imaging of tumors *in vivo*

We next explored the feasibility to use the <sup>131</sup>I-G5.NHAc-HPAO-PEG-FA dendrimers for targeted tumor SPECT imaging *in vivo*. After intravenous injection of the <sup>131</sup>I-G5.NHAc-HPAO-PEG-FA dendrimers or <sup>131</sup>I-G5.NHAc-HPAO-*m*PEG dendrimers with a similar dose, the tumor-bearing mice were scanned using a clinical SPECT imaging system (Figure 4). The SPECT images of the tumor site do not display an obvious enhancement at 2 min, 30 min, 1 h, 2 h, 3 h, 4 h postinjection when compared with those before injection. At 6 h, 16 h, 24 h postinjection, the SPECT image of tumor site of mice injected with the targeted <sup>131</sup>I-G5.NHAc-HPAO-PEG-FA dendrimers is much brighter than that injected with the nontargeted <sup>131</sup>I-G5.NHAc-HPAO-*m*PEG dendrimers at the same time point (Figure 4a). The SPECT imaging performance was also confirmed by *ex-vivo* tumor SPECT imaging at 6 h and 24 h postinjection (Figure 4b). It is clear that the tumor of mice treated with the targeted <sup>131</sup>I-G5.NHAc-HPAO-PEG-FA dendrimers displays much brighter

SPECT signal intensity than that treated with the nontargeted  $^{131}\text{I}$ -G5.NHAc-HPAO-*m*PEG dendrimers at the same time point. It is interesting to note that the tumor SPECT signal of mice treated with the  $^{131}\text{I}$ -G5.NHAc-HPAO-*m*PEG dendrimers is much weaker at 24 h postinjection than at 6 h postinjection, implying that the nontargeted  $^{131}\text{I}$ -G5.NHAc-HPAO-*m*PEG dendrimers without FA are able to be rapidly metabolized and have different biodistribution. In contrast, the FA modification renders the  $^{131}\text{I}$ -G5.NHAc-HPAO-PEG-FA dendrimers with prolonged tumor retention time likely *via* FA-mediated active targeting, allowing for enhanced SPECT imaging of the tumors.

The  $^{131}\text{I}$ -labeling of the dendrimers also enabled the exploration of the biodistribution of the nanodevices (Figure S9, ESI). The relative SPECT signal intensity of different organs at 6 h and 24 h postinjection of the  $^{131}\text{I}$ -G5.NHAc-HPAO-PEG-FA and  $^{131}\text{I}$ -G5.NHAc-HPAO-*m*PEG dendrimers reveals that liver has the largest accumulation of the  $^{131}\text{I}$ -G5.NHAc-HPAO-PEG-FA dendrimers, while other organs such as brain, heart, lung, kidney, spleen, intestines, stomach, soft tissue and other organs have a relatively low uptake of the particles (Figure S9a). For the nontargeted  $^{131}\text{I}$ -G5.NHAc-HPAO-*m*PEG dendrimers, liver also has the largest uptake of the particles at 6 h postinjection and the uptake of the particles in liver and other organs such as kidney, spleen, intestines, and stomach decreases at 24 h postinjection (Figure S9b). This suggests that the nontargeted  $^{131}\text{I}$ -G5.NHAc-HPAO-*m*PEG dendrimers can be quickly cleared from the major organs. Importantly, the tumor SPECT signal can be clearly discerned at 6 and 24 h postinjection of the  $^{131}\text{I}$ -G5.NHAc-HPAO-PEG-FA dendrimers, highlighting the role played by the FA-mediated targeting.

#### Targeted tumor radiotherapy *in vivo*

Based on the excellent therapeutic property of  $^{131}\text{I}$  under  $\beta$ -ray emission, we next evaluated the potential to use the  $^{131}\text{I}$ -G5.NHAc-HPAO-PEG-FA dendrimers for targeted tumor radiotherapy *in vivo* (Figure 5a). Clearly, the tumor growth rate of mice injected with the  $^{131}\text{I}$ -G5.NHAc-HPAO-PEG-FA dendrimers is significantly slower than that of mice treated with saline,  $\text{Na}^{131}\text{I}$ , and  $^{131}\text{I}$ -G5.NHAc-HPAO-*m*PEG dendrimers without FA ( $p < 0.001$ ), with the tumor inhibition efficacy order of  $^{131}\text{I}$ -G5.NHAc-HPAO-PEG-FA dendrimers ( $8.78 \pm 2.30$  times)  $>$   $^{131}\text{I}$ -G5.NHAc-HPAO-*m*PEG dendrimers ( $17.16 \pm 6.34$  times)  $>$   $\text{Na}^{131}\text{I}$  ( $18.58 \pm 6.12$  times)  $>$  control ( $26.65 \pm 5.76$  times) after 21 days' treatment. In contrast, the treatments of the  $^{131}\text{I}$ -G5.NHAc-HPAO-*m*PEG,  $\text{Na}^{131}\text{I}$ , and saline do not have any significant difference in terms of the tumor growth rate ( $p > 0.05$ ). The enhanced tumor inhibition efficacy of the  $^{131}\text{I}$ -G5.NHAc-HPAO-PEG-FA dendrimers should be due to the FA-mediated targeting effect (also proven *via* SPECT imaging). It should be noted that the tumor inhibition efficacy is solely associated with the labeled radioactive  $^{131}\text{I}$ . The tumors treated with the G5.NHAc-HPAO-*m*PEG or G5.NHAc-HPAO-PEG-FA dendrimers without  $^{131}\text{I}$  labeling display similar tumor growth rate to the saline control (Figure S10, ESI). The radiotherapy efficacy of the tumor mice was further demonstrated by the survival rate data (Figure 5b). It is clear that the mice treated with the  $^{131}\text{I}$ -G5.NHAc-HPAO-PEG-FA dendrimers maintain a 25% survival rate after 38 days, while 100% mice are dead when treated with saline after 22 days,  $\text{Na}^{131}\text{I}$  after 28 days, and  $^{131}\text{I}$ -

G5.NHAc-HPAO-*m*PEG dendrimers after 31 days, respectively. The survival rate data show that the treatment of the  $^{131}\text{I}$ -G5.NHAc-HPAO-PEG-FA dendrimers is most effective in prolong the lifetime of the tumor-bearing mice, further demonstrating the enhanced radiotherapeutic efficacy of the  $^{131}\text{I}$ -G5.NHAc-HPAO-PEG-FA dendrimers. Additionally, the treatments of the  $^{131}\text{I}$ -G5.NHAc-HPAO-*m*PEG,  $^{131}\text{I}$ -G5.NHAc-HPAO-PEG-FA, G5.NHAc-HPAO-*m*PEG and G5.NHAc-HPAO-PEG-FA dendrimers do not appear to largely change the body weight of the mice, similar to saline group (Figure S11, ESI). This suggests that the dendrimer carrier and radioactive  $^{131}\text{I}$ -labeled dendrimers are potentially nontoxic to the mice.

The tumor inhibition efficacy was also proven *via* H&E and TUNEL staining (Figure 6). H&E staining (Figure 6a) shows that different from the saline control and the G5.NHAc-HPAO-*m*PEG and G5.NHAc-HPAO-PEG-FA groups that display well-shaped tumor cells without the necrosis region, apparent necrosis can be found in the tumors treated with free  $\text{Na}^{131}\text{I}$ , nontargeted  $^{131}\text{I}$ -G5.NHAc-HPAO-*m*PEG dendrimers, and targeted  $^{131}\text{I}$ -G5.NHAc-HPAO-PEG-FA dendrimers. The tumor necrosis area follows the order of  $^{131}\text{I}$ -G5.NHAc-HPAO-PEG-FA dendrimers  $>$   $^{131}\text{I}$ -G5.NHAc-HPAO-*m*PEG dendrimers  $>$  free  $\text{Na}^{131}\text{I}$ . This suggests that with the FA-mediated targeting, the  $^{131}\text{I}$ -G5.NHAc-HPAO-PEG-FA dendrimers are able to be specifically accumulated in the tumor region, allowing for both targeted SPECT imaging and effective radiotherapy of the tumors.

The tumor inhibition efficacy of the developed  $^{131}\text{I}$ -G5.NHAc-HPAO-PEG-FA dendrimers was further evaluated by TUNEL assay.<sup>60</sup> As shown in Figure 6b, the tumors treated with the saline, G5.NHAc-HPAO-*m*PEG and G5.NHAc-HPAO-PEG-FA without  $^{131}\text{I}$  labeling only display scattered positive staining of apoptotic cells. In sharp contrast, the positive staining area of the apoptotic cells in the tumor sections follows the order of  $^{131}\text{I}$ -G5.NHAc-HPAO-PEG-FA  $>$   $^{131}\text{I}$ -G5.NHAc-HPAO-*m*PEG  $>$  free  $\text{Na}^{131}\text{I}$ . This can be further quantitatively confirmed by assessing cell apoptosis rate (the percentage of TUNEL-positive cells) (Figure 7), where the cell apoptosis rate follows the order of  $\text{Na}^{131}\text{I}$  (28.5%)  $<$   $^{131}\text{I}$ -G5.NHAc-HPAO-*m*PEG (45.8%)  $<$   $^{131}\text{I}$ -G5.NHAc-HPAO-PEG-FA (73.8%), significantly higher than the saline group (5.11%,  $p < 0.001$ ). Taken together, the H&E and TUNEL staining results suggest that the  $^{131}\text{I}$ -G5.NHAc-HPAO-PEG-FA dendrimers are able to exert enhanced tumor inhibition efficacy *via* both cell necrosis and cell apoptosis.

To assess the potential *in vivo* toxicity of the developed  $^{131}\text{I}$ -G5.NHAc-HPAO-PEG-FA dendrimers, the major organs (heart, liver, spleen, lung, and kidney) of the survived mice after treatment with saline, G5.NHAc-HPAO-*m*PEG, G5.NHAc-HPAO-PEG-FA,  $\text{Na}^{131}\text{I}$ ,  $^{131}\text{I}$ -G5.NHAc-HPAO-*m*PEG and  $^{131}\text{I}$ -G5.NHAc-HPAO-PEG-FA, respectively was H&E stained (Figure 8). We do not see noticeable organ damage and appreciable abnormality for all the treatment groups, similar to the saline control. Our results indicate that the developed  $^{131}\text{I}$ -G5.NHAc-HPAO-PEG-FA dendrimers potentially do not exert any *in vivo* toxic effects to mice.

#### Conclusion

To conclude, we developed a convenient approach to synthesizing multifunctional  $^{131}\text{I}$ -G5.NHAc-HPAO-PEG-FA

dendrimers for targeted tumor SPECT imaging and radiotherapy. Via the versatile dendrimer nanotechnology, multifunctional dendrimers modified with HPAO moieties can be effectively labeled with radioactive  $^{131}\text{I}$  with high radiochemical purity and good radio stability. Thanks to the FA-mediated targeting, the formed multifunctional  $^{131}\text{I}$ -G5.NHAc-HPAO-PEG-FA dendrimers are able to be used as an effective platform for targeted SPECT imaging and radiotherapy of an FAR-overexpressing xenografted tumor model *in vivo*. The strategy to use the facile dendrimer nanotechnology may be extended to develop various multifunctional radioactive dendrimeric nanopatform for targeted SPECT imaging and radiotherapy of different types of cancer.

## Acknowledgements

This research is financially supported by the National Natural Science Foundation of China (21273032, 81171368), the Ph.D. Programs Foundation of Ministry of Education of China (20130075110004), the Funds for the International Cooperation and Exchange of the National Natural Science Foundation of China (81381340177), the Program for Professor of Special Appointment (Eastern Scholar) at Shanghai Institutions of Higher Learning, and the Shanghai Municipal Commission of Health and Family Planning (20134y160). J. Z. thanks the support from the Chinese Universities Scientific Fund (BCZD201503).

## Notes and references

<sup>a</sup> State Key Laboratory for Modification of Chemical Fibers and Polymer Materials, College of Materials Science and Engineering, Donghua University, Shanghai 201620, People's Republic of China

<sup>b</sup> Department of Nuclear Medicine, Shanghai General Hospital, School of Medicine, Shanghai Jiaotong University, Shanghai 200080, People's Republic of China. E-mail: zhaojinhua1963@126.com

<sup>c</sup> College of Chemistry, Chemical Engineering and Biotechnology, Donghua University, Shanghai 201620, People's Republic of China. E-mail: xshi@dhu.edu.cn

<sup>d</sup> Experiment Center, Shanghai General Hospital, School of Medicine, Shanghai Jiaotong University, Shanghai 200080, People's Republic of China

<sup>1</sup> Jingyi Zhu and Lingzhou Zhao contributed equally to this work.

† Electronic supplementary information (ESI) available: Part of experimental details and additional experimental results.

- R. P. Baum, D. Hellwig and M. Mezzetti, *Q. J. Nucl. Med. Mol. Imag.*, 2004, **48**, 119-142.
- J. R. Buscombe, B. Holloway, N. Roche and E. Bombardier, *Q. J. Nucl. Med. Mol. Imag.*, 2004, **48**, 109-118.
- M. Hamoudeh, M. A. Kamleh, R. Diab and H. Fessi, *Adv. Drug Deliv. Rev.*, 2008, **60**, 1329-1346.
- S. Sergieva, T. Hadjieva, M. Doldurova, S. Stefanova and A. Dudov, *J. BUON*, 2006, **11**, 511-518.
- H. Hricak, D. J. Brenner, S. J. Adelstein, D. P. Frush, E. J. Hall, R. W. Howell, C. H. McCollough, F. A. Mettler, M. S. Pearce, O. H. Suleiman, J. H. Thrall and L. K. Wagner, *Radiology*, 2011, **258**, 889-905.
- K. A. Johnson, S. Minoshima, N. I. Bohnen, K. J. Donohoe, N. L. Foster, P. Herscovitch, J. H. Karlawish, C. C. Rowe, M. C. Carrillo,

D. M. Hartley, S. Hedrick, V. Pappas and W. H. Thies, *J. Nucl. Med.*, 2013, **54**, 476-490.

- C. C. Wagner and O. Langer, *Adv. Drug Deliv. Rev.*, 2011, **63**, 539-546.
- Y. Wu, Y. Sun, X. Zhu, Q. Liu, T. Cao, J. Peng, Y. Yang, W. Feng and F. Li, *Biomaterials*, 2014, **35**, 4699-4705.
- T. J. Wadas, E. H. Wong, G. R. Weisman and C. J. Anderson, *Chem. Rev.*, 2010, **110**, 2858-2902.
- K. R. Bhushan, P. Misra, F. Liu, S. Mathur, R. E. Lenkinski and J. V. Frangioni, *J. Am. Chem. Soc.*, 2008, **130**, 17648-17649.
- W. Ma, F. Kang, Z. Wang, W. Yang, G. Li, X. Ma, G. Li, K. Chen, Y. Zhang and J. Wang, *Amino Acids*, 2013, **44**, 1337-1345.
- B. B. Chin, Y. Nakamoto, J. W. M. Bulte, M. F. Pittenger, R. Wahl and D. L. Kraitchman, *Nucl. Med. Commun.*, 2003, **24**, 1149-1154.
- J. H. Kim, J.-H. Baek, J. S. Lee and I. Y. Hyun, *Clin. Nucl. Med.*, 2013, **38**, 904-907.
- J. F. W. Nijssen, G. C. Krijger and A. D. v. h. Schip, *Anti-Cancer Agents Med. Chem.*, 2007, **7**, 271-290.
- S. L. Pimlott and A. Sutherland, *Chem. Soc. Rev.*, 2011, **40**, 149-162.
- D. Emfietzoglou, K. Kostarelos and G. Sgouros, *J. Nucl. Med.*, 2001, **42**, 499-504.
- H.-E. Wang, H.-M. Yu, Y.-C. Lu, N.-N. Heish, Y.-L. Tseng, K.-L. Huang, K.-T. Chuang, C.-H. Chen, J.-J. Hwang, W.-J. Lin, S.-J. Wang, G. Ting, J. Whang-Peng and W.-P. Deng, *Nucl. Instrum Methods Phys. Res. Sect. A-Accel. Spectrom. Dect. Assoc. Equip.*, 2006, **569**, 533-537.
- K. F. Koral, Y. Dewaraja, J. Li, Q. A. Lin, D. D. Regan, K. R. Zasadny, S. G. Rommelfanger, I. R. Francis, M. S. Kaminski and R. L. Wahl, *J. Nucl. Med.*, 2003, **44**, 457-464.
- Y. K. Dewaraja, M. J. Schipper, P. L. Roberson, S. J. Wilderman, H. Amro, D. D. Regan, K. F. Koral, M. S. Kaminski and A. M. Avram, *J. Nucl. Med.*, 2010, **51**, 1155-1162.
- H.-W. Kao, Y.-Y. Lin, C.-C. Chen, K.-H. Chi, D.-C. Tien, C.-C. Hsia, M.-H. Lin and H.-E. Wang, *Bioorg. Med. Chem. Lett.*, 2013, **23**, 3180-3185.
- S. Banerjee, M. R. A. Pillai and N. Ramamoorthy, *Semin. Nucl. Med.*, 2001, **31**, 260-277.
- Q. Chen, K. Li, S. Wen, H. Liu, C. Peng, H. Cai, M. Shen, G. Zhang and X. Shi, *Biomaterials*, 2013, **34**, 5200-5209.
- R. Guo, H. Wang, C. Peng, M. Shen, L. Zheng, G. Zhang and X. Shi, *J. Mater. Chem.*, 2011, **21**, 5120-5127.
- H. Liu, H. Wang, R. Guo, X. Cao, J. Zhao, Y. Luo, M. Shen, G. Zhang and X. Shi, *Polym. Chem.*, 2010, **1**, 1677-1683.
- H. Liu, Y. Xu, S. Wen, Q. Chen, L. Zheng, M. Shen, J. Zhao, G. Zhang and X. Shi, *Chem. -Eur. J.*, 2013, **19**, 6409-6416.
- H. Liu, Y. Xu, S. Wen, J. Zhu, L. Zheng, M. Shen, J. Zhao, G. Zhang and X. Shi, *Polym. Chem.*, 2013, **4**, 1788-1795.
- C. Peng, K. Li, X. Cao, T. Xiao, W. Hou, L. Zheng, R. Guo, M. Shen, G. Zhang and X. Shi, *Nanoscale*, 2012, **4**, 6768-6778.
- C. Peng, L. Zheng, Q. Chen, M. Shen, R. Guo, H. Wang, X. Cao, G. Zhang and X. Shi, *Biomaterials*, 2012, **33**, 1107-1119.
- H. Wang, L. Zheng, C. Peng, R. Guo, M. Shen, X. Shi and G. Zhang, *Biomaterials*, 2011, **32**, 2979-2988.
- H. Wang, L. Zheng, C. Peng, M. Shen, X. Shi and G. Zhang, *Biomaterials*, 2013, **34**, 470-480.

31. S. Wen, K. Li, H. Cai, Q. Chen, M. Shen, Y. Huang, C. Peng, W. Hou, M. Zhu, G. Zhang and X. Shi, *Biomaterials*, 2013, **34**, 1570-1580.
32. Y. Wang, R. Guo, X. Cao, M. Shen and X. Shi, *Biomaterials*, 2011, **32**, 3322-3329.
33. M. Zhang, R. Guo, Y. Wang, X. Cao, M. Shen and X. Shi, *Int. J. Nanomed.*, 2011, **6**, 2337-2349.
34. X. Shi, I. Lee, X. Chen, M. Shen, S. Xiao, M. Zhu, J. R. Baker, Jr. and S. H. Wang, *Soft Matter*, 2010, **6**, 2539-2545.
35. Z. Qiao and X. Shi, *Prog. Polym. Sci.*, 2015, **44**, 1-27.
36. M. Shen and X. Shi, *Nanoscale*, 2010, **2**, 1596-1610.
37. L. Kong, C. S. Alves, W. Hou, J. Qiu, H. Mohwald, H. Tomas and X. Shi, *ACS Appl. Mater. Interfaces*, 2015, **7**, 4833-4843.
38. H. Liu, H. Wang, Y. Xu, R. Guo, S. Wen, Y. Huang, W. Liu, M. Shen, J. Zhao, G. Zhang and X. Shi, *ACS Appl. Mater. Interfaces*, 2014, **6**, 6944-6953.
39. J. Zhu and X. Shi, *J. Mater. Chem. B*, 2013, **1**, 4199-4211.
40. Y. Zheng, F. Fu, M. Zhang, M. Shen, M. Zhu and X. Shi, *Med. Chem. Commun.*, 2014, **5**, 879-885.
41. L. Zheng, J. Zhu, M. Shen, X. Chen, J. R. Baker, Jr., S. H. Wang, G. Zhang and X. Shi, *Med. Chem. Commun.*, 2013, **4**, 1001-1005.
42. J. Y. Zhu, L. F. Zheng, S. H. Wen, Y. Q. Tang, M. W. Shen, G. X. Zhang and X. Y. Shi, *Biomaterials*, 2014, **35**, 7635-7646.
43. Y. Zhang, Y. Sun, X. Xu, X. Zhang, H. Zhu, L. Huang, Y. Qi and Y.-M. Shen, *J. Med. Chem.*, 2010, **53**, 3262-3272.
44. J. M. Criscione, L. W. Dobrucki, Z. W. Zhuang, X. Papademetris, M. Simons, A. J. Sinusas and T. M. Fahmy, *Bioconjugate Chem.*, 2011, **22**, 1784-1792.
45. W. Cui, Y. Zhang, X. Xu and Y.-M. Shen, *Med. Chem.*, 2012, **8**, 727-731.
46. A. G. Khosroshahi, M. Amanlou, O. Sabzevari, F. J. Daha, M. R. Aghasadeghi, M. Ghorbani, M. S. Ardestani, M. S. Alavidjeh, S. M. Sadat, M. H. Pouriayevali, L. Mousavi and S. E. S. Ebrahimi, *Curr. Med. Chem.*, 2013, **20**, 123-133.
47. C. Kojima, Y. Niki, M. Ogawa and Y. Magata, *Int. J. Pharm.*, 2014, **476**, 164-168.
48. X. Xu, Y. Zhang, X. Wang, X. Guo, X. Zhang, Y. Qi and Y.-M. Shen, *Bioorg. Med. Chem.*, 2011, **19**, 1643-1648.
49. Y. Zhang, Y. Sun, X. Xu, H. Zhu, L. Huang, X. Zhang, Y. Qi and Y.-M. Shen, *Bioorg. Med. Chem. Lett.*, 2010, **20**, 927-931.
50. D. A. Tomalia and J. M. J. Frechet, *Dendrimers and Other Dendritic Polymers*, John Wiley & Sons Ltd, New York, 2001.
51. U. Avcibasi, H. Demiroglu, M. Ediz, H. A. Akalin, E. Ozcaliskan, H. Senay, C. Turkcan, Y. Ozcan, S. Akgol and N. Avcibasi, *J. Label. Compd. Radiopharm.*, 2013, **56**, 708-716.
52. J. Chen, S. Zhu, L. Tong, J. Li, F. Chen, Y. Han, M. Zhao and W. Xiong, *BMC Cancer*, 2014, **14**.
53. J. Zhu, Z. Xiong, M. Shen and X. Shi, *RSC Adv.*, 2015, **5**, 30286-30296.
54. J. Li, Y. He, W. Sun, Y. Luo, H. Cai, Y. Pan, M. Shen, J. Xia and X. Shi, *Biomaterials*, 2014, **35**, 3666-3677.
55. J. Li, L. Zheng, H. Cai, W. Sun, M. Shen, G. Zhang and X. Shi, *Biomaterials*, 2013, **34**, 8382-8392.
56. I. G. Campbell, T. A. Jones, W. D. Foulkes and J. Trowsdale, *Cancer Res.*, 1991, **51**, 5329-5338.
57. J. F. Ross, P. K. Chaudhuri and M. Ratnam, *Cancer*, 1994, **73**, 2432-2443.
58. Y.-J. Lu, K.-C. Wei, C.-C. M. Ma, S.-Y. Yang and J.-P. Chen, *Colloid Surf. B-Biointerfaces*, 2012, **89**, 1-9.
59. H. Yao, S. S. Ng, W. O. Tucker, Y.-K.-T. Tsang, K. Man, X.-m. Wang, B. K. C. Chow, H.-F. Kung, G.-P. Tang and M. C. Lin, *Biomaterials*, 2009, **30**, 5793-5803.
60. Z. Zhou, B. Kong, C. Yu, X. Shi, M. Wang, W. Liu, Y. Sun, Y. Zhang, H. Yang and S. Yang, *Sci. Rep.*, 2014, **4**, 3653.

---

**Figure captions**

**Figure 1.** Schematic illustration of the synthesis of the  $^{131}\text{I}$ -G5.NHAc-HPAO-PEG-FA dendrimers.

**Figure 2.** MTT viability assay of C6 cells after treatment with the G5.NHAc-HPAO-PEG-FA dendrimers at different concentrations for 24 h (Mean  $\pm$  SD, n = 3).

**Figure 3.** Confocal microscopy images of C6-HAR and C6-LFAR cells treated with the G5.NHAc-FI-HPAO-*m*PEG or G5.NHAc-FI-HPAO-PEG-FA dendrimers at a concentration of 1000 nM for 2 h, respectively.

**Figure 4.** SPECT images of the nude mice bearing C6 xenografted tumors at different time points post intravenous injection of the  $^{131}\text{I}$ -G5.NHAc-HPAO-PEG-FA and  $^{131}\text{I}$ -G5.NHAc-HPAO-*m*PEG dendrimers (tumor site was marked by white circle) (a) and SPECT images of *ex-vivo* tumors (b).

**Figure 5.** (a) The growth of C6 xenografted tumors after various treatments. The relative tumor volume was normalized according to their initial tumor volume (Mean  $\pm$  SD, n = 5). (b) The survival rate of C6 tumor-bearing mice after various treatments (Mean  $\pm$  SD, n = 5).

**Figure 6.** Representative H&E staining (a) and TUNEL assay (b) of C6 xenografted tumors treated with saline, G5.NHAc-HPAO-*m*PEG, G5.NHAc-HPAO-PEG-FA,  $\text{Na}^{131}\text{I}$ ,  $^{131}\text{I}$ -G5.NHAc-HPAO-*m*PEG and  $^{131}\text{I}$ -G5.NHAc-HPAO-PEG-FA, respectively. The scale bar shown in the H&E staining and TUNEL assay represents 100  $\mu\text{m}$ .

**Figure 7.** TUNEL-positive percentage of tumor cells measured by TUNEL assay.

**Figure 8.** H&E-stained tissue sections of major organs including heart, liver, spleen, lung and kidney from survived mice treated with saline, G5.NHAc-HPAO-*m*PEG, G5.NHAc-HPAO-PEG-FA,  $\text{Na}^{131}\text{I}$ ,  $^{131}\text{I}$ -G5.NHAc-HPAO-*m*PEG and  $^{131}\text{I}$ -G5.NHAc-HPAO-PEG-FA, respectively for 21 days. The scale bar represents 100  $\mu\text{m}$ .

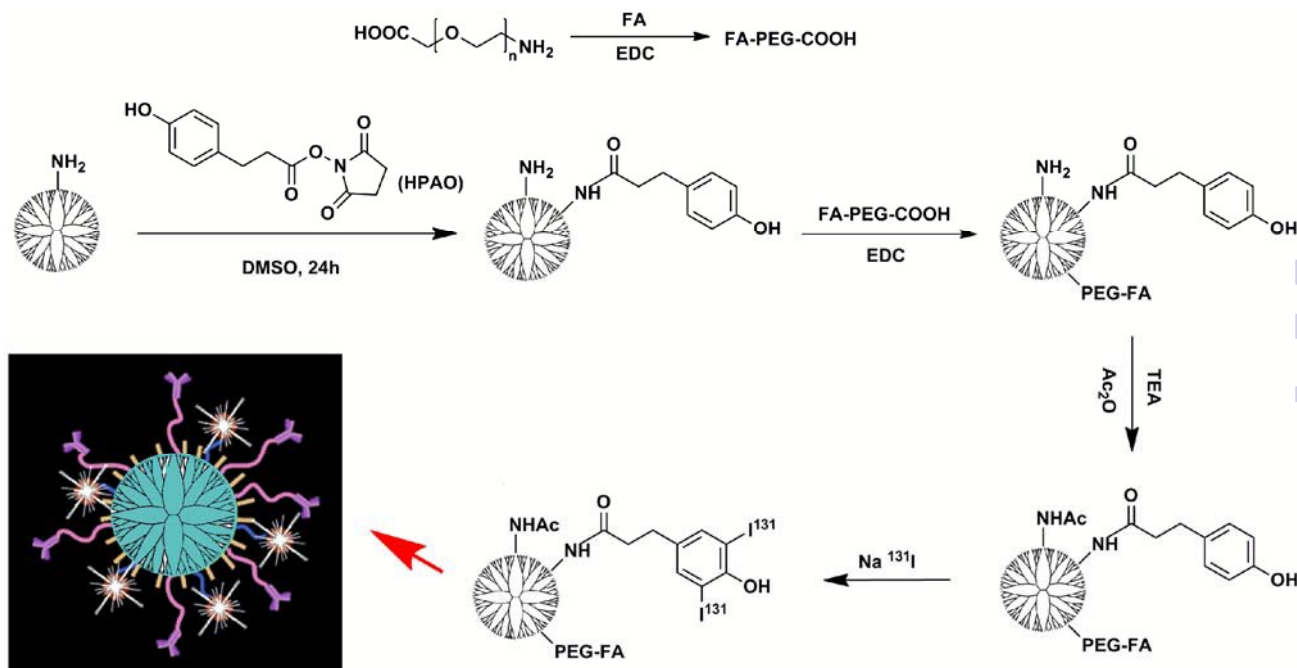
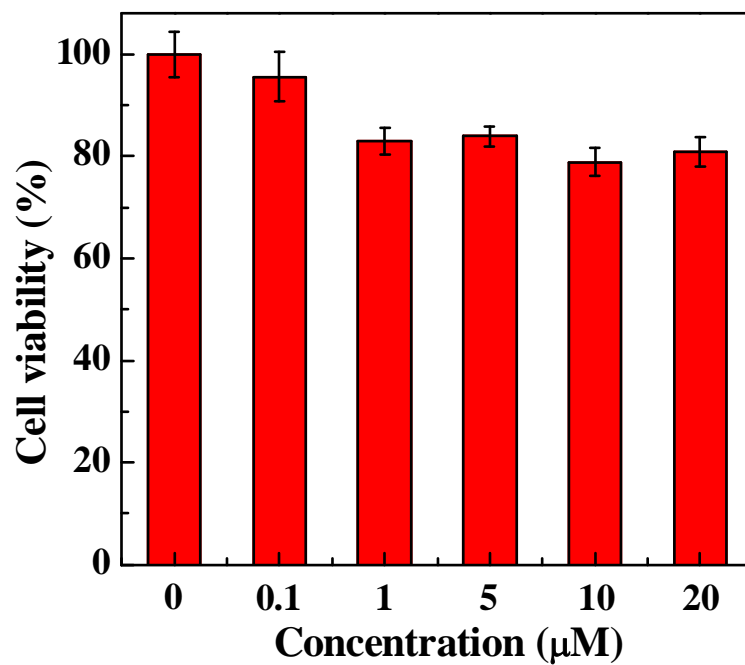


Figure 1

Zhu *et al.*



**Figure 2**

**Zhu *et al.***

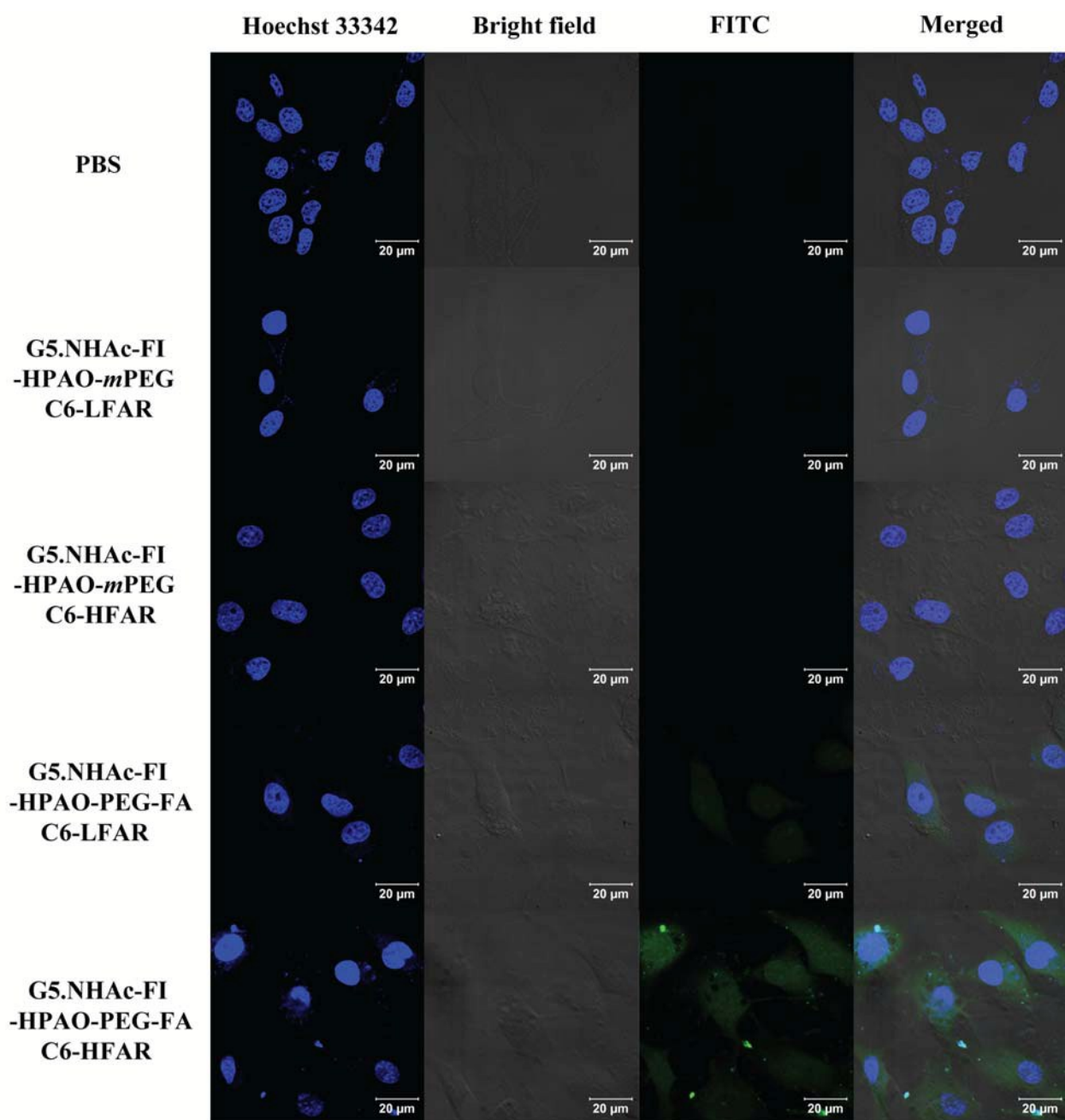


Figure 3

Zhu *et al.*

Nanoscale Accepted Manuscript

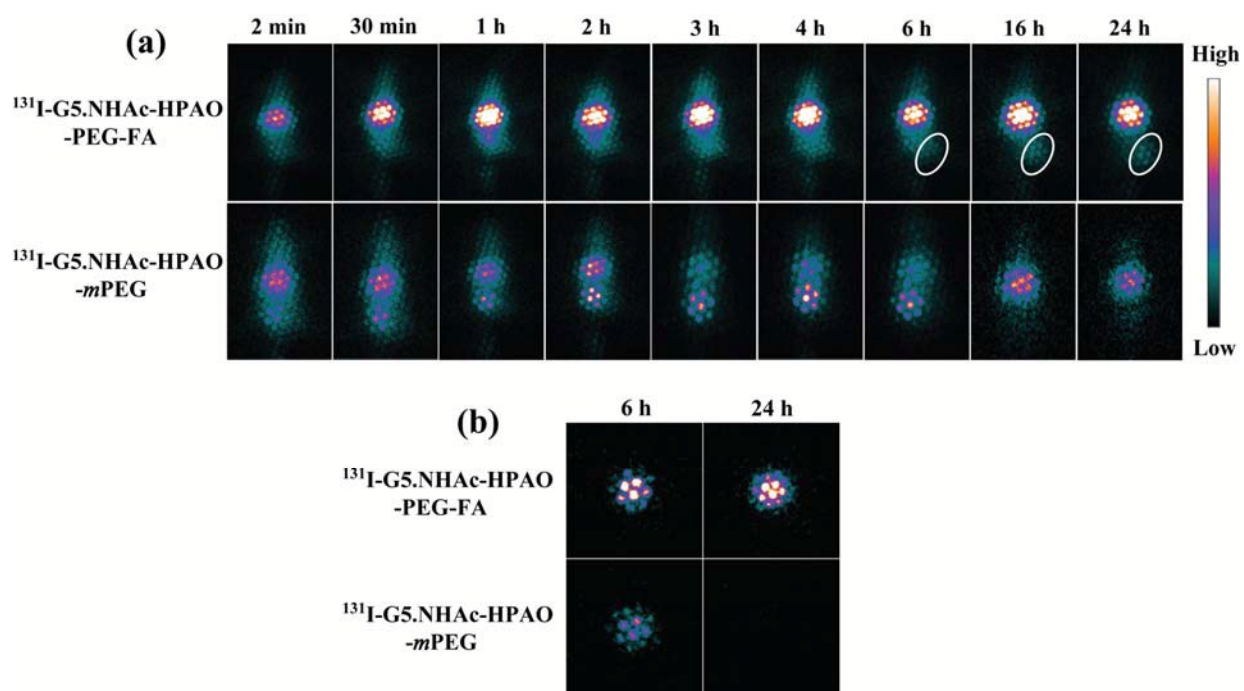


Figure 4

Zhu *et al.*

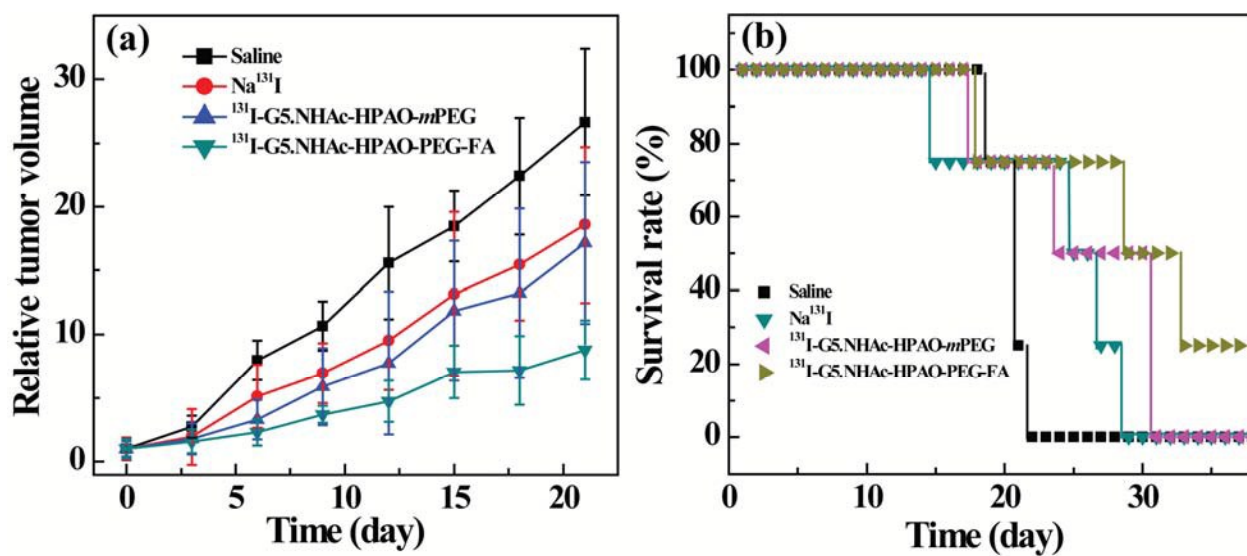
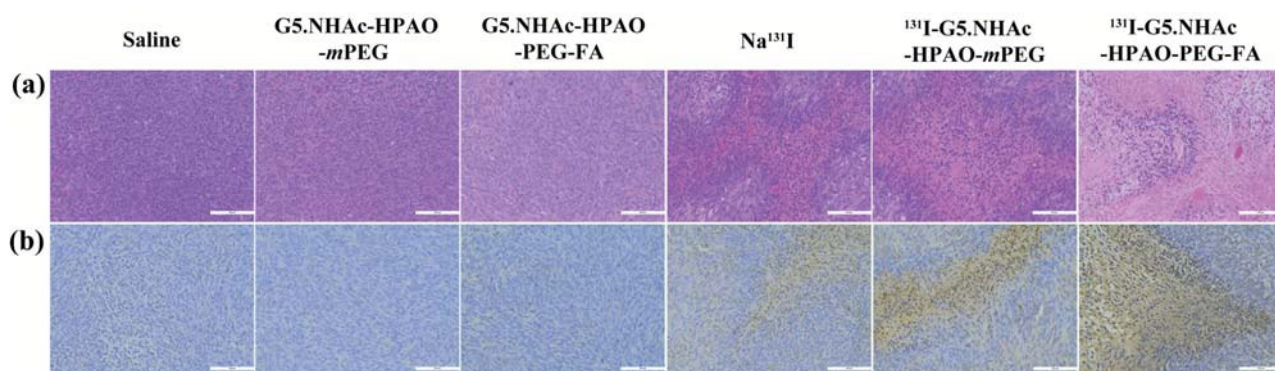


Figure 5

Zhu *et al.*

**Figure 6***Zhu et al.*

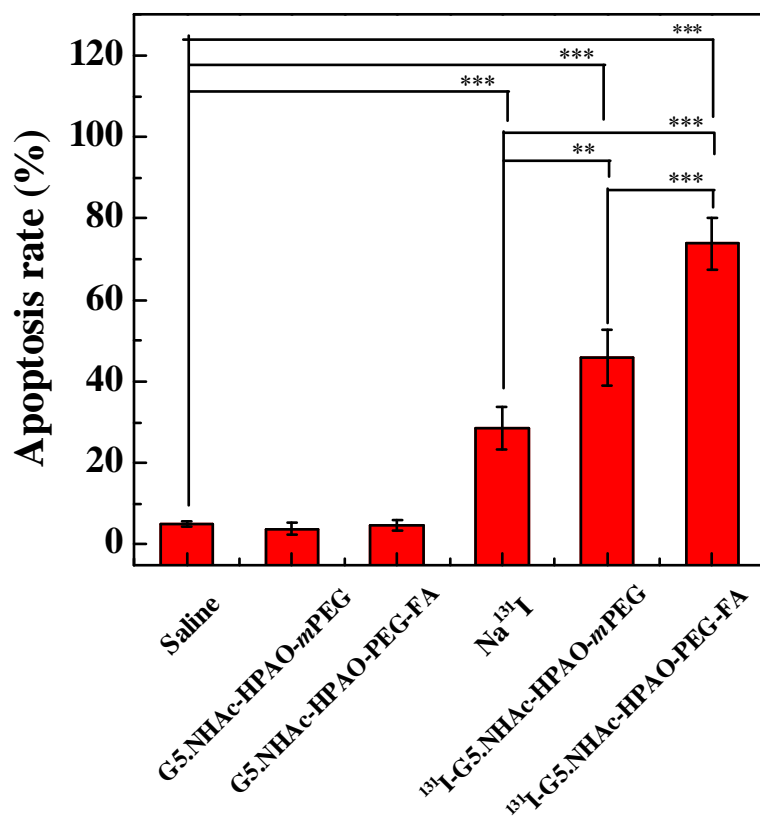


Figure 7

Zhu *et al.*

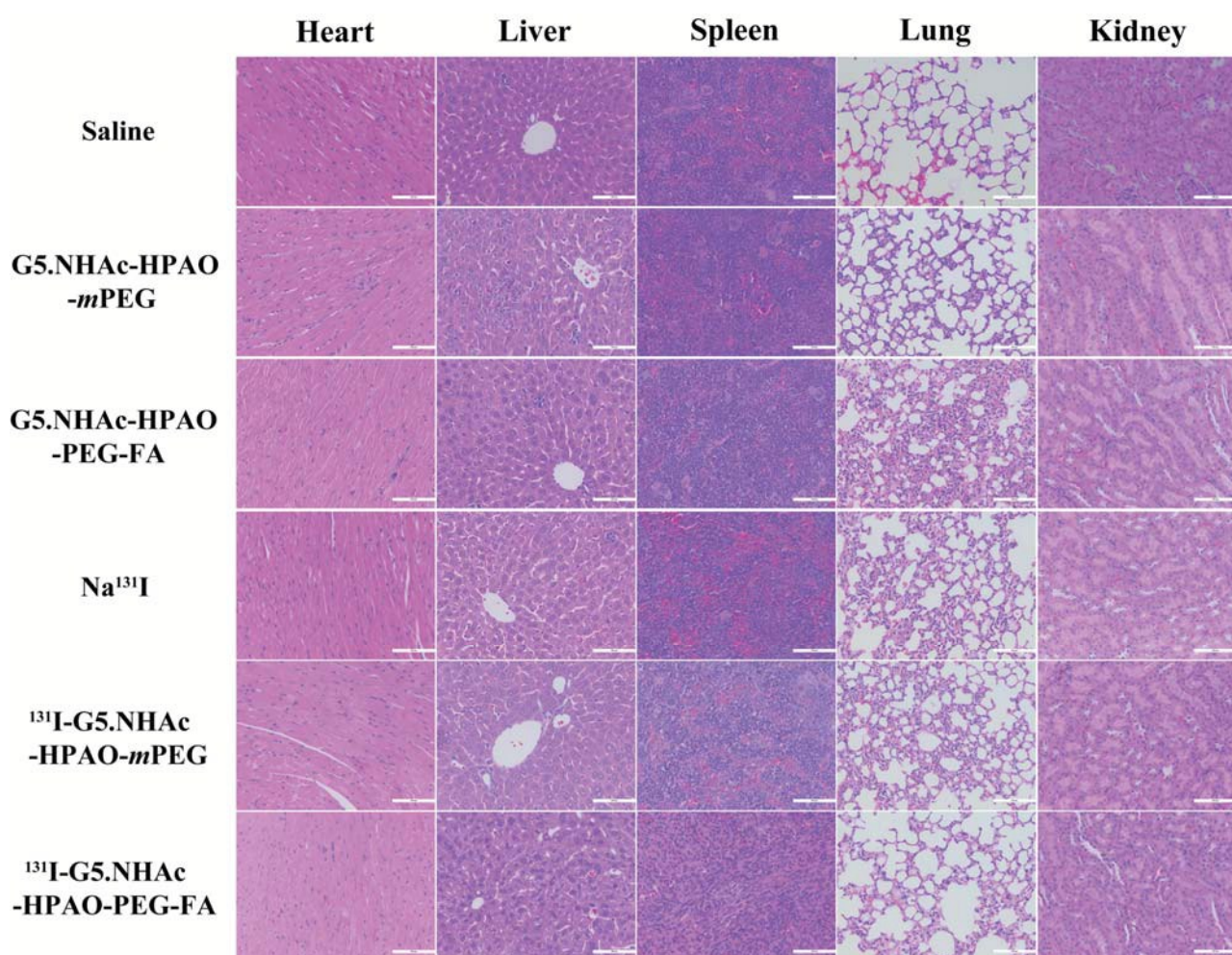


Figure 8

Zhu *et al.*